

# Progressive Retinal Degeneration Increases Cortical Response Latency of Light Stimulation but Not of Electric Stimulation

Beomseo Koo<sup>1,2</sup> and James D. Weiland<sup>1-3</sup>

<sup>1</sup> Department of Biomedical Engineering, University of Michigan, Ann Arbor, MI, USA

<sup>2</sup> Biointerfaces Institute, University of Michigan, Ann Arbor, MI, USA

<sup>3</sup> Department of Ophthalmology and Visual Sciences, University of Michigan, Ann Arbor, MI, USA

**Correspondence:** James D. Weiland, 2800 Plymouth Road, Building 36 Room G151, Ann Arbor, Michigan 48109-2800, USA. e-mail: [weiland@umich.edu](mailto:weiland@umich.edu)

**Received:** October 5, 2021

**Accepted:** March 31, 2022

**Published:** April 21, 2022

**Keywords:** retinitis pigmentosa; transcorneal electric stimulation; electrically evoked responses; visually evoked potentials; retinal prosthesis

**Citation:** Koo B, Weiland JD. Progressive retinal degeneration increases cortical response latency of light stimulation but not of electric stimulation. *Transl Vis Sci Technol.* 2022;11(4):19. <https://doi.org/10.1167/tvst.11.4.19>

**Purpose:** The brain is known to change functionally and structurally in response to blindness, but less is known about the effects of restoration of cortical input on brain function. Here, we present a preliminary study to observe alterations in visual and electrical evoked cortical potentials as a function of age in a clinically relevant animal model of retinitis pigmentosa.

**Methods:** We recorded brain potentials elicited by light (visual evoked potentials [VEPs]) or corneal electrical stimulation (electrical evoked response [EER]) in retinal degenerate animal model LE-P23H-1. We used a linear mixed model to examine the effects of age on latency and amplitude of VEP and EER age groups P120, P180, and P360.

**Results:** VEP N1, P1, and N2 latency and amplitude were analyzed across animal age. For 1 Hz VEP, N1 latency increased significantly with animal age (slope =  $0.053 \pm 0.020$  ms/day,  $P < 0.01$ ). For 10 Hz VEP, N1, P1, and N2 latency increased significantly with animal age (slope =  $0.104 \pm 0.011$ ,  $0.135 \pm 0.011$ ,  $0.087 \pm 0.023$  ms/day, and  $P < 0.001$  for all VEP peaks). Conversely, EER latency did not change with age. Signal amplitude of VEP or EER did not change with age.

**Conclusions:** Cortical potentials evoked by electrical stimulation of the retina do not diminish in spite of continued retinal degeneration in P23H rats.

**Translational Relevance:** These findings suggest that retinal bioelectronic treatments of retinitis pigmentosa will activate cortex consistently despite variations in outer retinal degeneration. Clinical studies of retinal stimulation should consider varying retinitis pigmentosa genotypes as part of the experimental design.

## Introduction

Blindness and visual impairment are major public health concerns.<sup>1</sup> Given the reliance on vision to travel and interact with the physical world, vision loss is associated with lowered independence and quality of life.<sup>1</sup> Retinitis pigmentosa (RP; a collective term for a heterogenous inherited retinopathy) has a prevalence of 1 in 4000 patients worldwide, and often results in severe vision loss.<sup>2,3</sup> Of the few treatment options available, bioelectronic methods, such as retinal prosthesis and transcorneal electric stimulation (TES), are currently of interest. Retinal prostheses can

partially restore vision and TES may slow degeneration progression. Retinal prostheses electrically stimulate the remaining retinal cells to create artificial vision in patients with RP.<sup>4</sup> With these implants, patients can locate large objects and improve mobility.<sup>3,5</sup> TES therapy, such as the CE-marked Okuvision,<sup>6-9</sup> provides a noninvasive therapeutic stimulation treatment for RP. By regularly inducing upregulation of neurotrophic factors,<sup>10,11</sup> TES therapy works to counteract the apoptotic events in the retina. TES preclinical studies showed clear visual field maintenance,<sup>10</sup> photoreceptor layer maintenance,<sup>11,12</sup> and visual acuity improvements<sup>10</sup> in study animals. However, the method has variable clinical results.

With no single cure to RP's umbrella of over 200 distinct genetic mutations, both retinal prosthesis and TES are still relevant potential treatment options for RP.

Clinical studies of patients with ocular interventions to improve their vision revealed modifications of cortical structure and function. Cataract removal surgery increased the secondary visual cortex volume when observed under magnetic resonance imaging (MRI)<sup>13</sup> and showed a positive correlation of pre- and postoperative spontaneous superior parietal lobule activity and calcarine gray matter volume.<sup>14</sup> Preliminary functional MRI studies showed that ARGUS II Retinal Prosthesis users, after 6 months of prosthesis use ( $n = 3$ ), experienced increased lateral geniculate nucleus and visual cortex blood oxygen level-dependent (BOLD) signal from light stimulus.<sup>15</sup> However, the final level of the BOLD signal in implanted individuals are not as high as those with normal vision, which may be due to irreversible changes from retinal degeneration. Traditionally, the adult brain is considered to have lower potential for structural plasticity than the developing brain, but functional plasticity still can occur rapidly.<sup>16</sup> Consequently, late-stage RP functionally remodels the sensory cortices.<sup>15,17–19</sup> The V1 retinotopic activity is altered in late-stage RP; a degeneration-dependent shift where the central retinal input is routed toward peripheral vision locations in V1.<sup>17</sup> Functional MRI revealed significantly lower V1 spontaneous activity, and different V1 BOLD activity during tactile tasks for late-stage RP.<sup>15,18,19</sup> The degree to which the visual cortex can adapt to artificial stimuli will be an important factor determining the success of retinal prostheses. Thus, the possibility of retinal degeneration precluding visual cortex availability to process prosthetic stimuli is an important issue to be investigated.

Therapeutic electrical stimulation for RP has renewed interest, based in part on the finding of a neurotrophic effect related to corneal stimulation and subretinal prosthesis.<sup>12,20</sup> Studies on the multicenter Okuvision's clinical test trial cohort ( $n = 105$ ) generally report positive results of chronic stimulation in visual function tests and safety.<sup>6–9</sup> However, there is still variability within the results of various TES studies. Small effects or inconclusive effects in visual function within the study cohort does not support an adoption of TES in the entire RP population. The variability may result from not knowing the specific genetic mutation of RP within participants,<sup>7</sup> collection of subjective data,<sup>7</sup> and small variation between data collection methods between study centers. To date, no brain imaging studies in TES for patients with RP have been done.

The clinical studies described above are limited in part by an incomplete characterization and control of the patient background.<sup>6</sup> Given the limitations (recruitment and variability) typical in human studies, animal studies with reduced variability have a role in providing complementary information on visual cortex response to electrical stimulation. Animal models of retinal degeneration are well-accepted means to study retinal and cortical response to degeneration.<sup>10,11,21–23</sup> The P23H mutation of RP, where a proline to histidine substitution in the rhodopsin gene causes protein misfolding-led metabolic dystrophy in photoreceptor endoplasmic reticulum, has been well characterized in its modality of retinal degeneration.<sup>20,24</sup> P23H is disproportionately represented in human RP, with 41% of rhodopsin mutation cases identified as P23H even though it is only one of 13 known rhodopsin mutations that cause autosomal-dominant RP, which represents about a third of the entire RP cases.<sup>25,26</sup> Due to this high relevance to human disease, the P23H rat model has documented photoreceptor degeneration that correlate with diminishing electroretinogram (ERG) amplitude and increasing latency.<sup>21,24,27</sup> P23H has been used in multiple preclinical studies for experimental therapies.<sup>10,28–30</sup>

Evoked cortical potentials recording in animal brain have aided the design of retinal prostheses,<sup>31–33</sup> but few studies have examined changes in cortical potentials during progressive levels of retinal degeneration. In this study, we measured cortical activity evoked by light and electrical stimuli as a function of progressive retinal degeneration in P23H rat up to 1 year of age. We compared latency and amplitude of visual evoked potentials (VEPs) to electrical evoked responses (EERs) and found that alterations in VEP, expected based on prior ERG studies in a P23H animal model,<sup>21,24,34</sup> were not present in the EERs, where the amplitude and latency did not change with progressive degeneration.

## Methods

### Animal Care and Use

Referred to as LE-P23H-1, pigmented heterozygote P23H-1 rats were chosen as they experience slower yet still complete retinal degeneration.<sup>21</sup> LE-P23H-1 rats of the P120, P180, and P360 age groups ( $n = 5, 6,$  and  $3$  at P120, P180, and P360, respectively) were used. The slower degeneration mimicked the degeneration human adults experienced with RP, allowing for assessment of TES benefit. Pigmented P23H-1 rats were bred

through the University of Michigan Unit for Laboratory Animal Medicine’s Animal Husbandry by crossing an autosomal-dominant Sprague Dawley with the P23H mutation (SD-Tg[P23H]1Lav homozygote [RRRC, USA]) with a Long-Evans rat (Charles River Laboratories, Inc. Wilmington, DE). Three Long-Evans rats at age P400 were used for optical coherence tomography imaging comparisons. All animal husbandry, surgical, and experimental procedures were approved by the Institutional Animal Care and Use Committee (IACUC) of the University of Michigan.

### Devices

The neural recording device consisted of stainless-steel screw electrodes, with a threaded portion with diameter and length of 1 and 2.7 mm (81.3206; Esslinger, USA), to circuit board assembly (Fig. 1). Each recording screw was soldered to a 32 AWG, stainless-steel wires with PFA insulation (791900; A-M Systems, Sequim, WA) with a connector pin (ED11335-ND; Digi-Key Electronics, Thief River Falls, MN). The corneal stimulation electrode consisted of a 32 AWG, platinum/iridium wire with PFA insulation

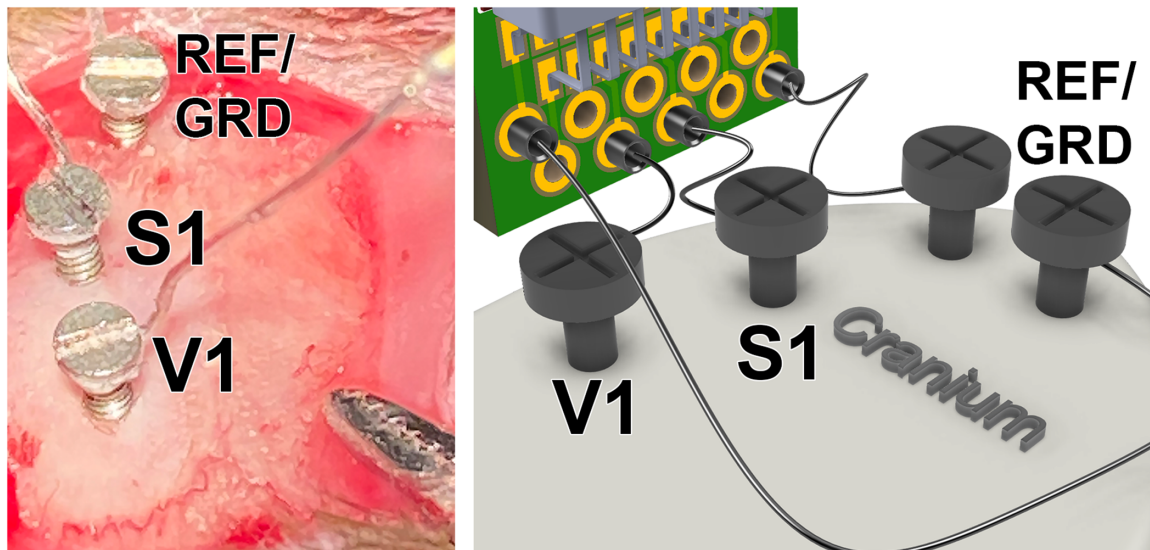
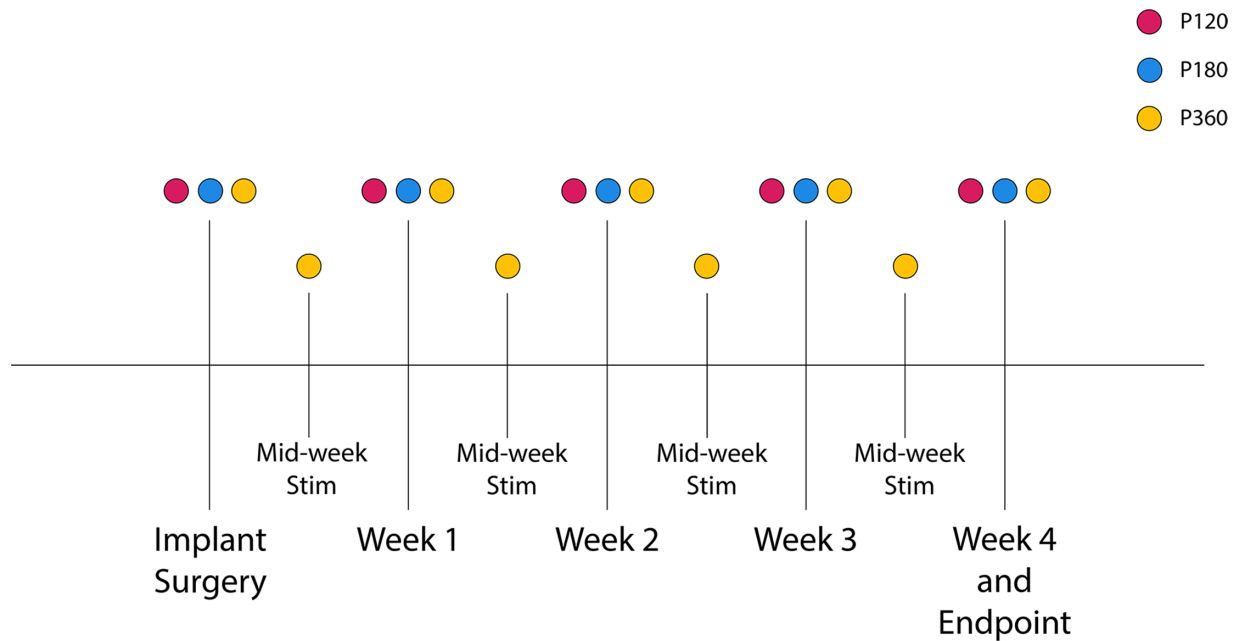


**Figure 1.** (Top) Experimental timeline, red = P23H P120, blue = P180, and yellow = P360. (Left) Example image of recording screws in place. (Right) Example render of recording screws connecting to circuit board assembly. GRD, recording ground; REF, recording reference; S1, somatosensory cortex; V1, primary visual cortex.

(778000; A-M Systems) looped to create a 3 mm diameter hoop that rested on the cornea and a 5 cm wire terminating in a connector pin (520200; A-M Systems).

## Surgery Procedure

LE-P23H-1 rats of the P120, P180, and P360 age groups ( $n = 5, 6, \text{ and } 3$  at P120, P180, and P360, respectively) were implanted 4 weeks before the target age with recording screws. Aseptic surgery techniques were used, all surgical tools were sterilized with an autoclave, and implants were sterilized with ethylene-oxide. Animals were anesthetized initially with 3% isoflurane in a chamber and maintained at 1.5–3% isoflurane via a nose-cone attached to the stereotaxic system. The anesthetized animal was placed on a heating pad set at 37°C and the animal's head was fixed with ear bars. A muted hindlimb pinch response was measured and carprofen (5 mg/kg) was injected subcutaneously before surgical procedures. The head was shaved and then cleaned 3 times with betadine and 70% ethanol. A longitudinal incision was made at the dorsal surface of the animal's head, the fascia was removed, and the skull was dried. Excessive bleeding of the skull or surrounding skin was stymied with either hydrogen peroxide with a cotton tip applicator or drops of 2% lidocaine to constrict the blood vessels. Burr holes were created with a micromotor (Foredom, Bethel, CT) with a dental drill bit (HM2-008-HP; Meisinger USA, LLC, Centennial, CO) at the following coordinates relative to bregma: Anterior-Posterior Medial-Lateral, [2 2], [2 -2], and [-6.5 3] mm corresponding to ground, e, and V1, respectively. The recording screws were advanced into the burr holes, placing the screw's bottom surface approximately 0 to 150  $\mu\text{m}$  past the skull to limit contact and pressure on the neural tissue (see Fig. 1). The recording screws were anchored and insulated in dental acrylic (Lang Dental, Wheeling, IL). Triple antibiotic ointment (CURAD Medical Supplies, Northfield, IL) was applied on the surrounding tissue and the incision was sutured around the dental acrylic headcap with a 5-0 nylon suture (Ethicon USA, Somerville, NJ). Silver sulfadiazine cream (Ascend Laboratories, Parsippany, NJ) was applied at and around the surgical site to prevent infection. Immediately postoperative, the animal was kept on a heated blanket and monitored until ambulatory. The postsurgery monitoring included daily monitoring for 1 week, silver sulfadiazine application as needed, and carprofen analgesia coverage for 72 hours postsurgery.

## Electrochemical Impedance Spectroscopy

Electrochemical impedance spectroscopy (EIS) of recording screws were measured weekly for 4 weeks. Animals were anesthetized with a ketamine/xylazine cocktail (80 mg/kg and 8 mg/kg, respectively), injected intraperitoneal, and placed on a heating pad set at 37°C. The recording screws were connected to a Gamry Reference 600 system (Gamry Instruments, Warminster, PA). Two-electrode EIS was recorded using the following settings: 10 mV AC RMS and 1 Hz to 1 MHz frequency sweep. The implanted ground recording screw was used as the combined counter/ e electrode.

## Optical Coherence Tomography

Optical coherence tomography (OCT) images were obtained either at a week before the end point or at the end point. Animals were anesthetized with ketamine/xylazine cocktail (80 mg/kg and 8 mg/kg, respectively) injected intraperitoneal. Anesthetized animals received 1% tropicamide (Akorn, US) and 0.5% proparacaine (Akorn Inc., Amityville, NY) drops in both eyes and were left to rest for 5 minutes. The animal was placed on the Bioptigen 90-KIT-M/R Rodent Alignment System (Bioptigen, Inc., Morrisville, NC). The Envisu R2210 OCT system (Bioptigen, USA) was aligned so the optic nerve was center-of-frame and the reference arm was adjusted until the retina appeared flat. The eye was hydrated and cleaned with BSS drops until image capture. Then, 1000 B-scans of 1.6 mm depth and 2.6 mm length were captured to create a 2.6  $\times$  2.6  $\times$  1.6 mm image volume of the retina. The cross-section centered at the optic nerve was extracted and the image contrast was optimized for the retinal ganglion cell layer. Retinal layer thickness values were sampled in representative images about 300  $\mu\text{m}$  away from the optic nerve using the measurement tool in FiJi.<sup>35</sup> Total retinal thickness span from the retinal ganglion cell layer until the retinal pigment epithelium. The outer nuclear layer (ONL) was characterized as the dark space between the inner nuclear layer and the first bright line denoting the outer limiting membrane.<sup>21</sup> The inner segment (IS) layer was characterized as space between the first bright horizontal line past the outer nuclear layer (ONL) and the next bright line.<sup>36,37</sup> The outer segment (OS) layer was characterized as the horizontal line above the retinal pigment epithelium, which brightly defines the bottom layer of the retina in the OCT image, and the dark space above it until the IS layer.<sup>36,37</sup>

## Evoked Potential Recording

Any animals that experienced headcap removal were excluded. The P120 and P180 age groups received weekly light and electric stimulation sessions under ketamine/xylazine anesthesia (see Fig. 1). The P360 age group received twice weekly light and electric stimulation sessions, with alternating anesthesia of ketamine/xylazine and 1.5% maintained isoflurane (see Fig. 1). A twice-weekly ketamine regimen was considered, but animal health concerns related to animal age and weight led to limiting ketamine anesthesia frequency to once a week. The W2100 electrophysiology recording system includes a TTL-triggered timestamp module, which noted the stimulation event for the VEP and EER recordings.

### Visually Evoked Potentials

Anesthetized animals received 1% tropicamide and 0.5% proparacaine drops to the eye contralateral to the implanted V1 electrode ( $n = 5, 5, \text{ and } 3$  for P120, P180, and P360, respectively). The W2100-HS14-ES2-0.5 mA headstage (MCS Pharma, Hamburg, Germany) was connected to the animal. The animal was dark adapted for at least 5 minutes before recording. Before recording, a 9000K white LED (C5030-WAN-CCBEB151-ND; DigiKey, USA) was placed approximately 1.5 cm away from the dilated eye. The LED had a 181 mW/cm<sup>2</sup> steady-state ON irradiance measured using a photodiode sensor set at 535 nm, set 1.5 cm away from the LED (PM16-130; Thorlabs Inc., Newton, NJ). A drop of BSS was applied to the eye and siphoned with a surgical spear to hydrate and clean the eye before stimulation. If the eye was not readily proptosed (in the case of isoflurane anesthesia, rarely of ketamine/xylazine anesthesia), then a speculum (WPI, Worcester, MA) was used to retract the eyelids and expose the eye. Flash stimulation of the retina was done with 10 ms pulse duration of 1 or 10 Hz frequency, with 100 or 300 pulses, respectively. For a subset of animals, the eye ipsilateral to the implanted V1 electrodes were also stimulated as a negative control.

### Electrically Evoked Responses

Anesthetized animals received a drop of proparacaine to the eye contralateral to the implanted V1 electrode ( $n = 3, 2, \text{ and } 3$  for P120, P180, and P360, respectively). The MCS W2100-HS14-ES2-0.5 mA headstage was connected to the animal. A Pt/Ir wire loop was placed to rest lightly on the cornea surface, with electrical contact ensured by BSS, which was reapplied during the procedure. The return electrode was a stainless-steel wire placed between the tongue and cheek of the animal.<sup>10</sup> The stimulation and return

electrodes were connected to the PlexStim Electrical Stimulator System (Plexon, Dallas, TX). The animal was checked for proper anesthetized state and lack of blink response to additional BSS addition before stimulation. Electric stimulation parameters were cathodic-first pulses, 1 ms per phase, 2 Hz pulse rate with these incrementing amplitudes: 100, 200, 400, and 800  $\mu\text{A}$ . After the initial recording, a TES session was performed for 30 minutes, where an 800  $\mu\text{A}$ , cathodic-first, 1 ms per phase, 2 Hz pulse was applied for the duration (Figs. 2–4).<sup>10</sup> An oscilloscope displayed the stimulation voltage transient to verify stimulation electrode connection and integrity.

An additional EER recording was obtained at the end point, where anesthesia was increased to 5% isoflurane, effectively extinguishing cortical activity. The EERs at this anesthesia level were used as a negative control for electric stimulation as well as used in post-processing to reduce stimulation artifact present in the EER recordings, because the artifact was still present in these EERs. The animal was induced at 3% isoflurane, and upon reaching a sufficient plane of anesthesia, where hindlimb pinch response was nonexistent, the anesthesia was increased to 5% until breathing was reduced to approximately 0.33 to 0.5 breaths/second. Spontaneous neural activity and EER recording using an 800  $\mu\text{A}$  cathodic-first, 1 ms per phase, 2 Hz pulse were recorded in this state.

### Electrophysiology Processing

All neural recordings were converted to hdf5 format and export to MATLAB for processing. VEP recordings were passed through a digital Butterworth filter with a pass band of 10 to 80 Hz. EER recordings were passed through a digital Butterworth filter with a pass band of 1 to 300 Hz. Recording stacks, containing VEP or EER recording spanning -50 to 300 ms surrounding the stimulation event, were made using stimulation event timestamps in the VEP and EER recordings. A spontaneous neural activity recording stack was made using the same timestamps of its respective VEP or EER recording (Fig. 2). Similar to the feature extraction of neural spike recording,<sup>38,39</sup> stimulation event stacks were passed through k-means clustering ( $k = 14$ ). K-groups that contained <10% of the trials were rejected, to remove outlier stimulation events that may contain contamination from sources unrelated to stimulation. Recording stacks contained a max of 100 trials for 1 Hz VEP and 300 trials for 10 Hz VEP and EER, and k-means clustering removed an estimated 30% to 50% of trials in a 2-minute recording session. For EER recordings, -1.0 to 5.0 ms of the stimulation event was blanked, and the missing values were filled in with linear inter-

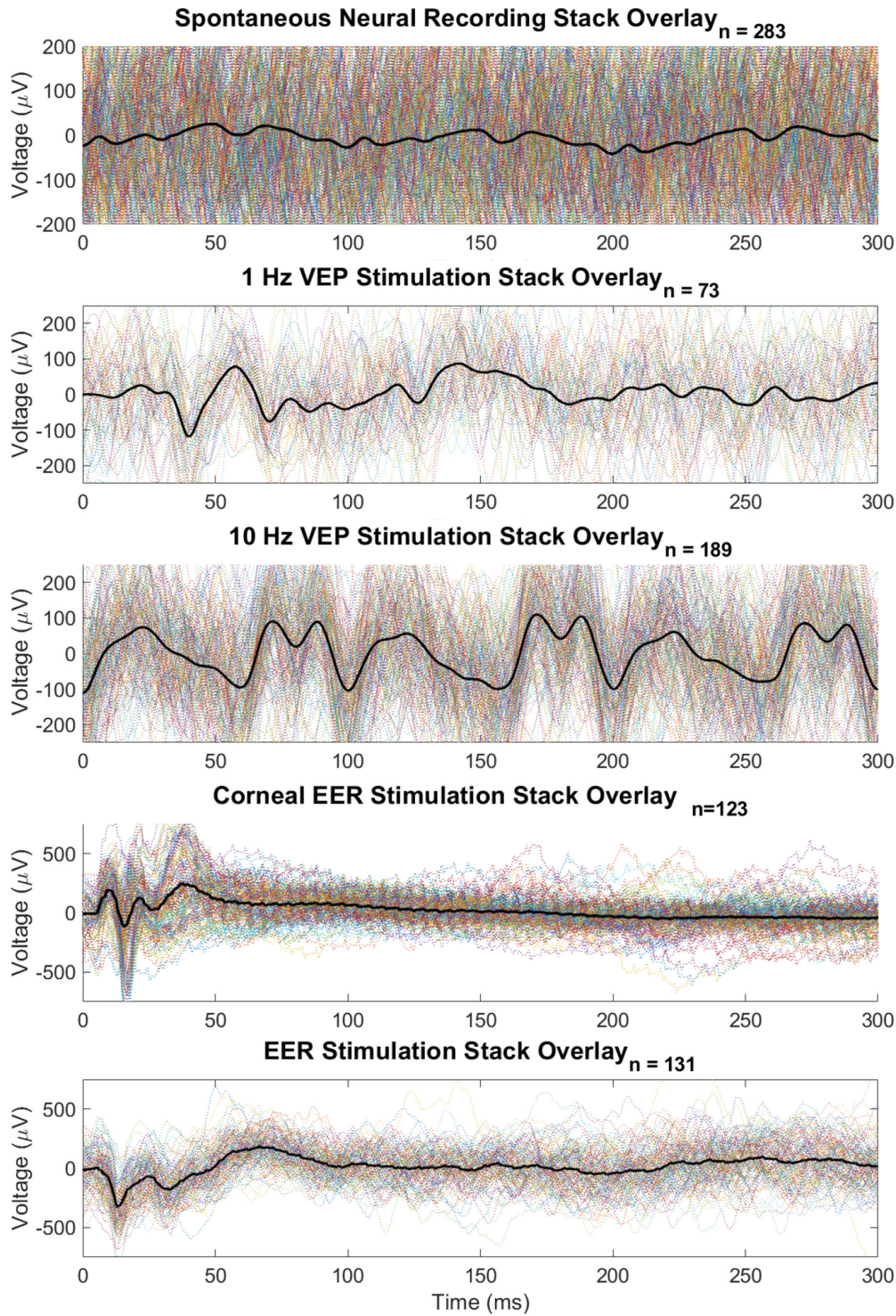


**Figure 2.** Representative electrophysiology traces of spontaneous neural activity, 1 Hz VEP (P180), 10 Hz VEP (P180), corneal EER recordings (P360), and retinal EER recording (P120). (Black) Mean trace of the stimulation event stack.  $n$  = number of stimulation event trials included in recording stack.

polation (Figs. 3, 4). Afterward, the average trace of the 5% isoflurane electric stimulation recording stack was overlaid with the averaged EER trace (see Fig. 3). To remove the exponential decay portion of the stimu-

lation artifact, a timepoint was designated manually where the decay initiates. Local minima or maxima peak was extracted for both the isoflurane and EER trace (see Fig. 3). The ratio of the two values was used

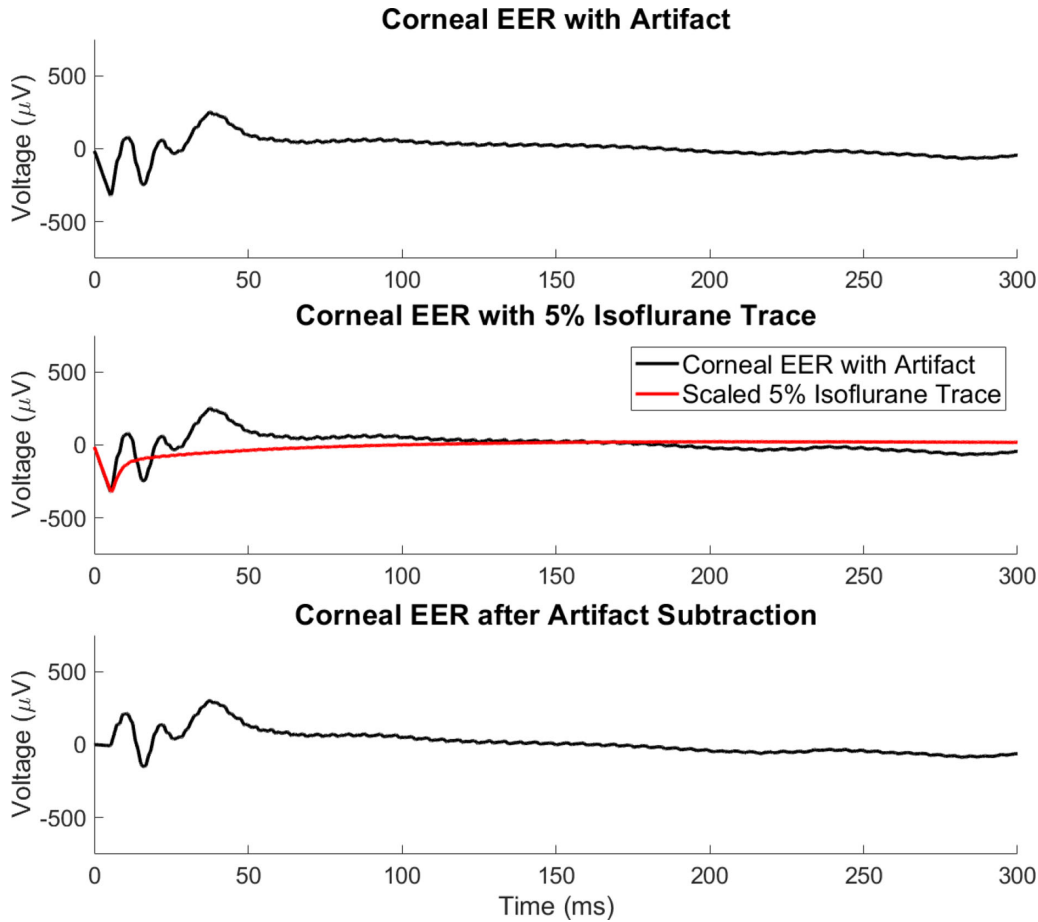


**Figure 3.** Representative averaged electrophysiology traces of corneal EER, scaled 5% isoflurane trace (red in second panel), and the resulting trace after the scaled 5% isoflurane trace is subtracted from the EER to remove stimulus artifacts.

to scale the isoflurane trace, normalizing the isoflurane trace to the EER recording. The scaled, averaged isoflurane trace was then subtracted from the EER stimulation event stack to mitigate the remaining stimulation artifact. The resulting VEP and EER stimulation recording stacks were used to calculate neural response latency (ms) and root-mean squared (RMS) values ( $\mu\text{V}$ ).

Latency for VEP and EER peaks were calculated semi-automatically using the averaged trace of the stimulation event stacks. Twice the RMS value of the averaged trace of the spontaneous neural activity recording stack was used as a threshold reference for the VEP and EER peaks. Spontaneous neural activity recording stacks were made using the same timestamps of the respective VEP or EER recording. In MATLAB, a user manually selected a possible negative or positive peak and the MATLAB function localmin or localmax extracted the latency of the local the nearest local minima or maxima peak. Peak distance values (in ms) were calculated using the absolute difference between the N1 and P1 peaks as well as the P1 and N2 peaks.

Trials that did not result in distinguishable VEP or EER peaks in the averaged trace were excluded.

RMS values of VEP, EER, and their respective spontaneous recordings were calculated as an indicator of signal strength. Stimulation event recording stacks were made with a reference window informed by the VEP and EER peak latency data. The windows used were: [20, 170], [20, 100], and [5, 90] ms for VEP 1 Hz, VEP 10 Hz, and EER, respectively. Spontaneous neural activity recording stacks were made using the same time intervals of the respective VEP or EER recording. RMS was calculated using the averaged trace of the recording stack of the VEP, EER, and their respective spontaneous recordings. RMS ratios were calculated by dividing the stimulation RMS value by the spontaneous RMS value. Trials that did not result in distinguishable VEP or EER peaks in the averaged trace were excluded.

### Retinal EER

For a subset of animals ( $n = 4$ ), an intraocular stimulation electrode was implanted at the same

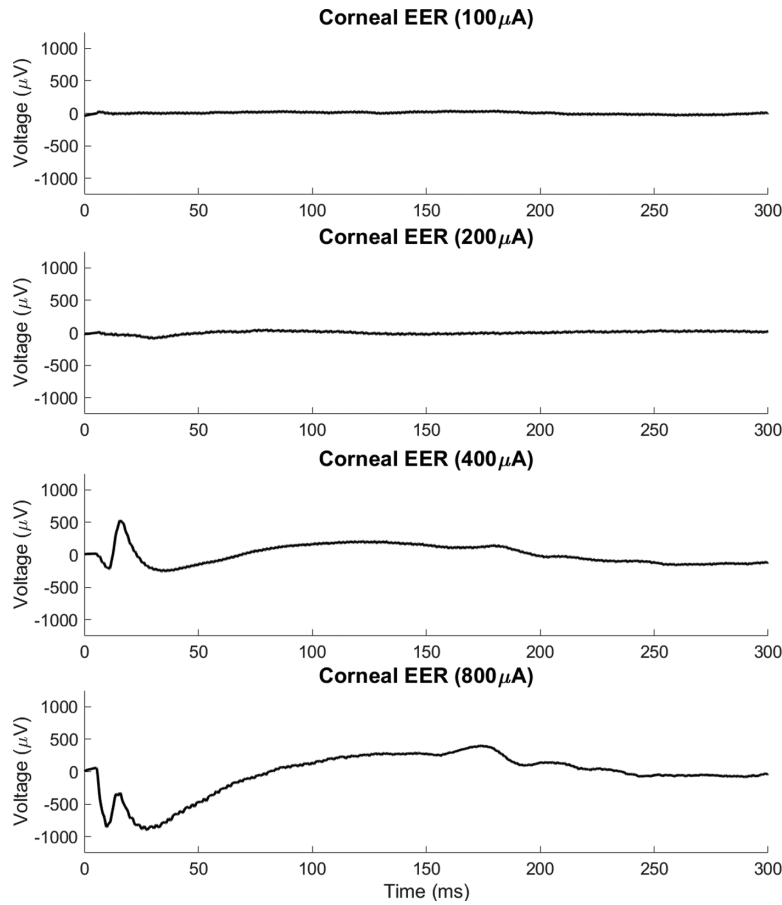


**Figure 4.** Representative averaged electrophysiology traces of corneal EER with incrementing stimulation current amplitudes.

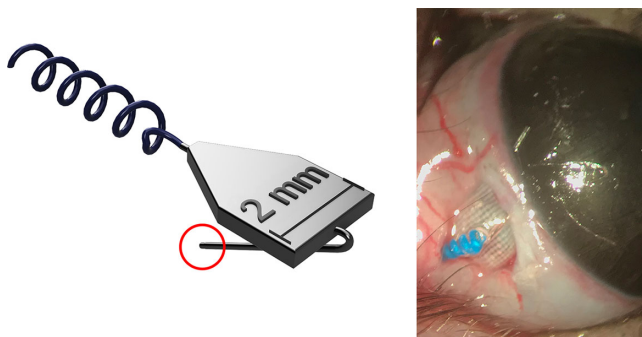


**Figure 5.** (Left) Three dimensional model of retinal implant. The stimulating electrode, 125  $\mu\text{m}$  Pt/Ir wire, circled in red. (Right) Example image of implant in place. The blue connecting wire is routed subcutaneously to the recording screws.

time as the neural recording screws (Fig. 5). The intraocular electrode consisted of a 125  $\mu\text{m}$  diameter Pt/Ir wire with PFA insulation embedded in a 3  $\times$  2 mm silicone sandwich (Micro-Leads, Somerville, MA), 3.25 mm of the wire used for intraocular insertion, and 3 cm coiled wire (Micro-Leads) terminating to a connector pin.

The animal implant protocol follows the same procedure mentioned above and adds extra steps for intraocular electrode insertion. Two drops of 0.5% proparacaine were applied to the implant eye, allowing 5 minutes of rest time for analgesic to take effect. A 5-0 silk suture fed through the eyelid was used to proptose the eye. An incision at the conjunctiva was made at the dorsal surface of the rat's eye using an iris scissors, and a blunt dissection with iris scissors exposed the underlying sclera. A 16G needle and a 12G needle was used to create a subcutaneous tunnel from the conjunctiva incision to the head incision, and the intraocular electrode was fed into the lumen of the 12G needle. The 12G needle was removed, leaving the intraocular electrode routed at the eye. A transscleral incision was made using a 30G needle. The intraocular wire was inserted, and the silicone sandwich anchored to the sclera with two 8-0 nylon suture ties. The conjunctiva flap was pulled over the electrode and closed using 8-0 nylon sutures.

EERs using the intraocular electrode were collected with 250  $\mu\text{A}$ , cathodic-first, 1 ms per phase, 2 Hz, biphasic pulses.

Maintenance of an adequately sized animal cohort of the intraocular wire with detectable EER for 4 weeks was inconsistent, which led us to abandon this group for statistical comparisons. However, some EER data using the intraocular electrode was obtained and can be used to compare to the corneal stimulation.

### Statistical Analysis

Latency, RMS, and RMS ratio were analyzed using a linear mixed-effects models in MATLAB (fitlme), using animal age in days as a fixed effect and animal ID as a random effect (model equation: latency ~ 1 + animal age + (1|animal ID)). The OCT layer thicknesses were also fitted to the same linear mixed-effects model, but animal age was inputted as categorical variables with Long-Evans P400 added as a comparison group. The reported regression slope value are the regression results with standard error. Animal age groups were also compared categorically (P120, P180, and P360) as a secondary measure with 1-way ANOVA to account for uneven sample sizes. The *P* values of the *t*-tests of linear mixed model and categorical comparisons were measured. Significance was defined at an alpha value of 0.05.

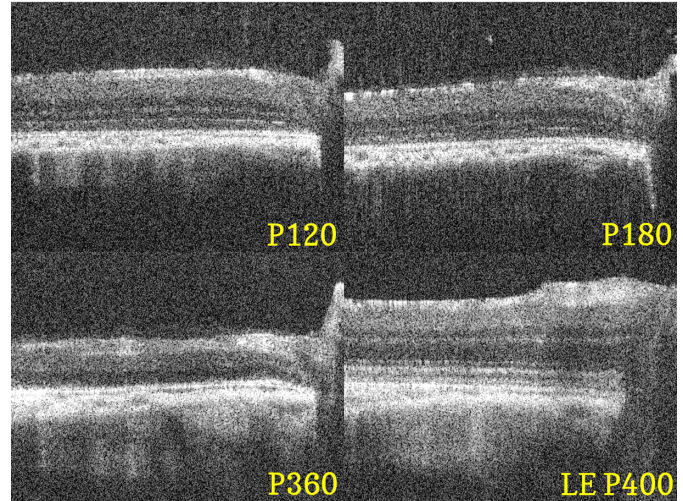


**Figure 6.** Representative OCT cross-section of the retina at different LE-P23H-1 age groups and of LE at P400. The optic nerve is oriented to the right of each panel.

euthanasia. Pupil dilation was confirmed visually, and each animal showed a clear cornea, no visible cataract, clear intravitreal space, and retinal visualization prior to stimulation.

### Retinal Condition During LE-P23H-1 Degeneration

Retinal degeneration progression was verified using imaging data centered at the optic nerve (Fig. 6). Total retinal thickness was significantly different for P120, P180, and P360 ( $P = 2.00e^{-08}$ ,  $3.40e^{-10}$ , and  $1.91e^{-12}$ , respectively) when compared with Long-Evans P400. OCT images sampled at P120 and P180 showed a progressive decrease in the ONL ( $P = 1.19e^{-08}$  and  $2.92e^{-09}$ , respectively) when compared to Long-Evans P400. The IS layer for P120 was observed as larger than Long-Evans P400 group ( $P = 0.03$ ). The OS was not detectable for P120 and P180 group (Table). The ONL,

## Results

### Experimental Model

Recording screws remained within operable impedance values (1–5 kΩ) over the 4-week implant period. Some brains at end point euthanasia showed “dimpling” where the recording screw unintentionally contacted the brain. However, no significant scar tissue encapsulation around the recording screws was observed during brain dissection after end point

**Table.** Quantitative Measurements Made From OCT Images.

	Long-Evans P400	P120	P180	P360
Animal count	3	5	5 <sup>a</sup>	6 <sup>b</sup>
Retinal thickness	120.34 ± 2.22	90.90 ± 1.43***	80.73 ± 4.88***	64.46 ± 4.65***
ONL	31.18 ± 0.60	14.68 ± 0.98***	10.96 ± 1.61***	N/A
IS	13.69 ± 1.26	16.47 ± 0.57*	11.65 ± 2.29	N/A
OS	16.98 ± 0.94	N/A	N/A	N/A

<sup>a</sup>One P180 rat was excluded due to poor OCT image quality.

<sup>b</sup>P360 OCT group includes 3 rats used for VEP/EER measurements and 3 additional rats, which were used in an anatomical study with no implantation or electrical stimulation.

\* =  $P < 0.05$ , \*\* =  $P < 0.01$ , \*\*\* =  $P < 0.001$ , the *P* value is from categorical regression from MATLAB linear mixed-effects model using Long-Evans P400 as the reference point.

N/A, not applicable.

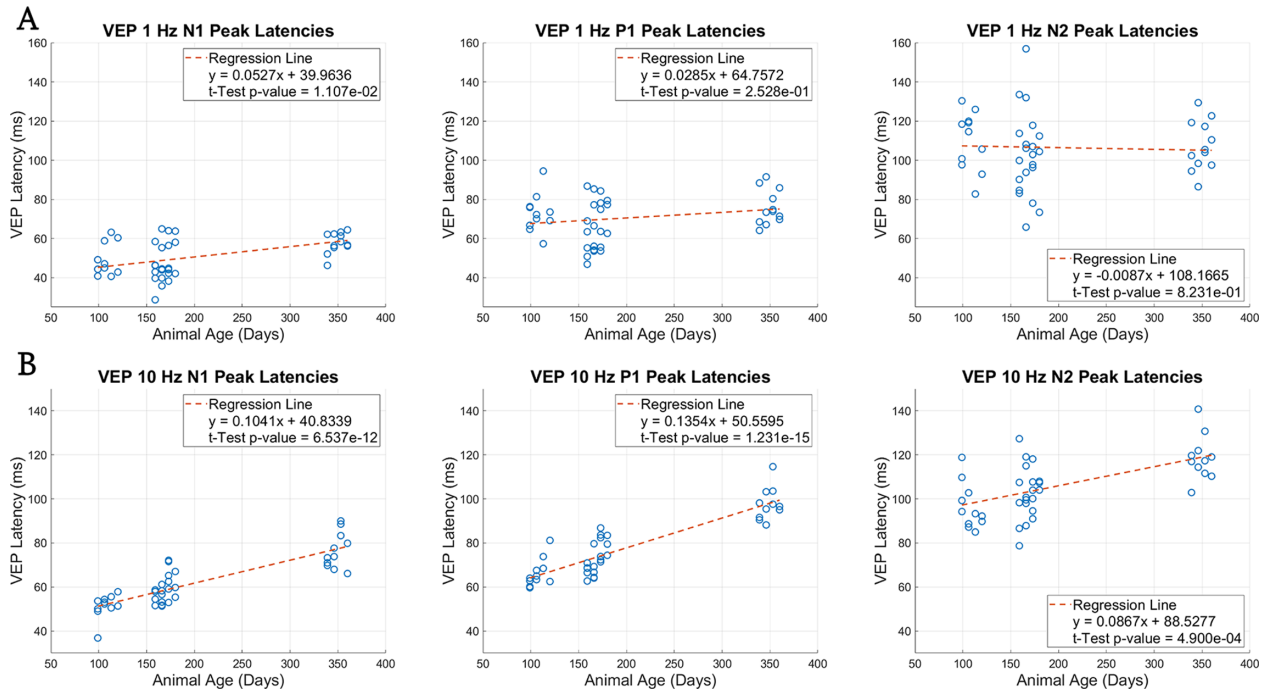


**Figure 7.** Plotted linear regression of VEP peak latency for (A) 1 Hz VEPs N1, P1, and N2 peaks and (B) 10 Hz VEPs N1, P1, and N2 peaks. Statistical  $\alpha = 5.0e^{-02}$  for significance. Red dotted line = linear regression result.

OS, and IS layers were undetectable for P360 age group (see the Table).

### Visually Evoked Potentials Reflect Retinal Degeneration

VEP waveforms were present in all animal age groups, including the P360 group. VEP waveform quality depended on averaging, because the screw electrodes were subject to noise and motion artifact. K-means extraction rejected k-groups that contained, in total, 30% to 50% of stimulation trials in a session, but these electrophysiology traces were produced in 2-minute increments and are highly replicable. VEP recording with stimulation to the ipsilateral eye resulted in a muted response compared to contralateral stimulation, which confirms that the VEP recordings are due to visual pathway activation.

VEP N1, P1, and N2 latency were analyzed across animal age. For 1 Hz stimulation, N1 latency of the VEP complex significantly increased across animal age (Fig. 7). For 10 Hz stimulation, all 3 latencies of the VEP complex significantly increased across animal age (see Fig. 7). In addition, the time between peaks for 10 Hz stimulation ( $P = 1.710e^{-3}$  for N1-P1 and  $P = 1.733e^{-2}$  for P1-N2) were significantly different across animal age (Fig. 8). Animal age affected 10 Hz VEP

latency (slope =  $0.104 \pm 0.011$ ,  $0.135 \pm 0.011$ , and  $0.087 \pm 0.023$  ms/day and  $P = 6.54e^{-12}$ ,  $1.23e^{-15}$ , and  $4.90e^{-04}$ , respectively, for N1, P1, and N2) more than 1 Hz latency (slope =  $0.053 \pm 0.020$ ,  $0.029 \pm 0.025$ , and  $0.009 \pm 0.039$  ms/day and  $P = 1.11e^{-02}$ , 0.253, and 0.823, respectively, for N1, P1, and N2).

RMS of 1 Hz, 10 Hz VEP recordings, and spontaneous neural recordings were measured (Fig. 9). RMS of 1 Hz or 10 Hz VEP stimulation trials did not change significantly across animal age. When compared categorically, RMS was only significantly different between P120 and P360 for 1 Hz only ( $P = 0.025$ ). However, RMS ratio did not change significantly across animal age or change significantly categorically. RMS compared categorically between the earliest measured timepoint P90 ( $n = 4$ , week 1 of the P120 group) and P360 ( $n = 2$ , week 4 of the P360 group) were not significant for both 1 Hz and 10 Hz VEP.

### Electrically Evoked Responses Dynamics are Independent of Retinal Degeneration

Stimulus current titration revealed successful EER detection in 400 and 800  $\mu A$  stimulation, with 800  $\mu A$  providing clearer potential peaks (see Fig. 4). Weekly 30-minute stimulation of the cornea at 100 to 800  $\mu A$

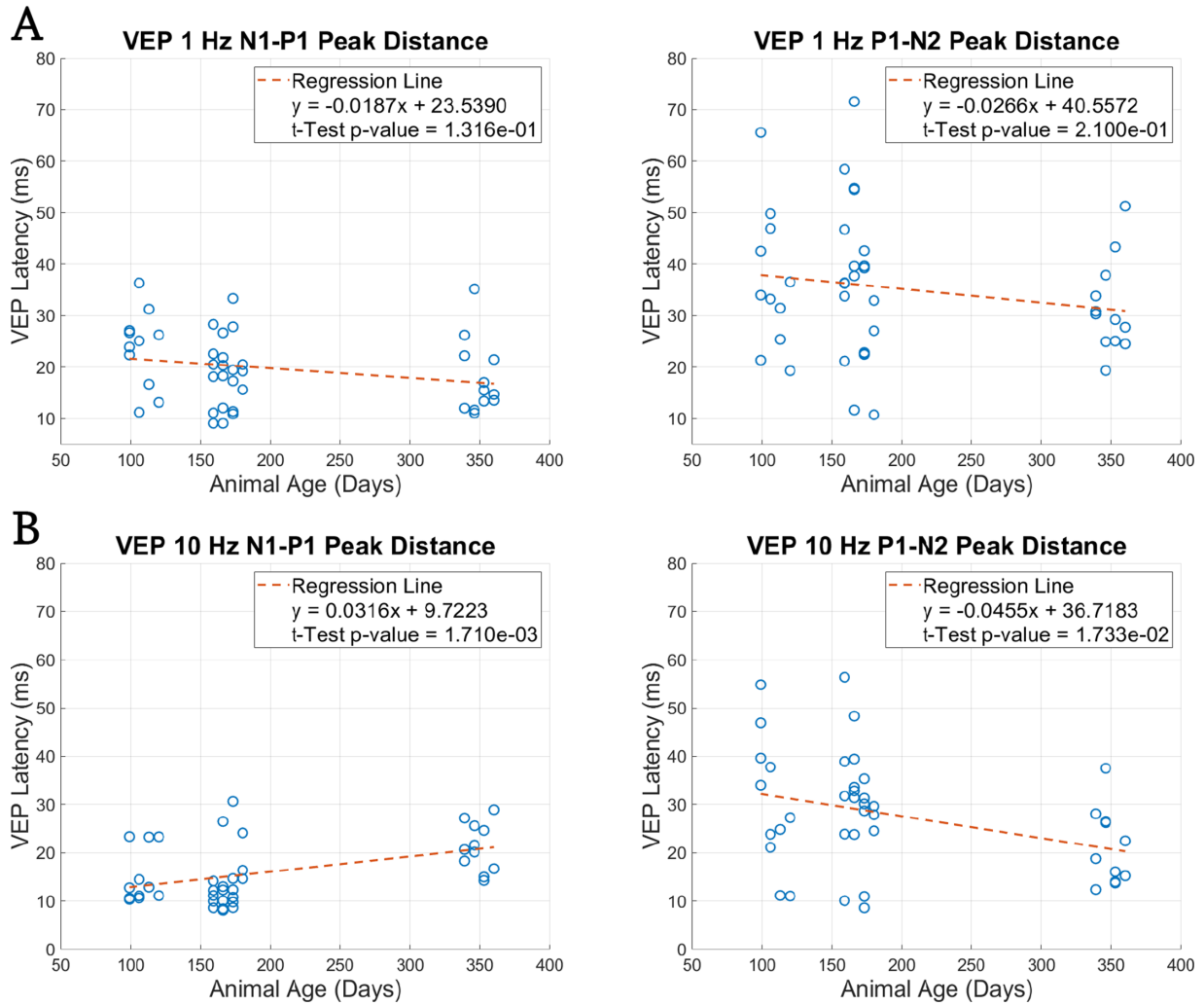


**Figure 8.** Plotted linear regression of VEP peak distance for (A) 1 Hz VEPs N1-P1 and P1-N2 peak distances and (B) 10 Hz VEPs N1-P1 and P1-N2 peak distances. Statistical  $\alpha = 5.0e^{-02}$  for significance.

did not cause any corneal damage. Comparing the retinal and corneal EER, the representative retinal EER peak latencies were 13.2, 25.3, and 33.0 ms for N1, P1, and N2, respectively, which were comparable to the mean peak latency of 11.8, 18.1, and 37.0 ms for corneal EER of age-matched P180 animals. The retinal EER recordings were obtained in two animals, so these results could not be analyzed rigorously, but they do provide supporting data that the corneal EER waveform was due to retinal activation. Similar EER latencies for rats were reported by others.<sup>33</sup>

Latency of EER recordings were measured. Latency of N1, P1, and N2 peaks were recorded from the averaged electrophysiology recording stacks (Fig. 10). Recorded EER peaks showed lower latency compared to their respective peaks in recorded VEPs. EER peak latency did not change significantly across animal age

(see Fig. 10; slope =  $0.0029 \pm 0.0065$ ,  $-0.0058 \pm 0.0016$ , and  $-0.0138 \pm 0.0222$  ms/day and  $P = 6.03e^{-01}$ ,  $2.15e^{-01}$ , and  $6.22e^{-01}$ , respectively, for N1, P1, and N2). EER peak latency showed no significant difference when compared categorically between animal age groups for all latency peaks.

RMS of EER recordings and spontaneous neural recordings were measured (Fig. 11). RMS is confounded by incomplete and inconsistent artifact removal, which results in large variation of this measurement. RMS and RMS ratio of corneal electric stimulation trials did not change significantly across animal age. RMS compared categorically shows P180 and P120 to be significantly different ( $P = 6.0e^{-03}$ ). RMS ratio compared categorically shows P180 to be significantly different from P120 ( $P = 2.1e^{-03}$ ) and P360 ( $P = 1.31e^{-02}$ ).

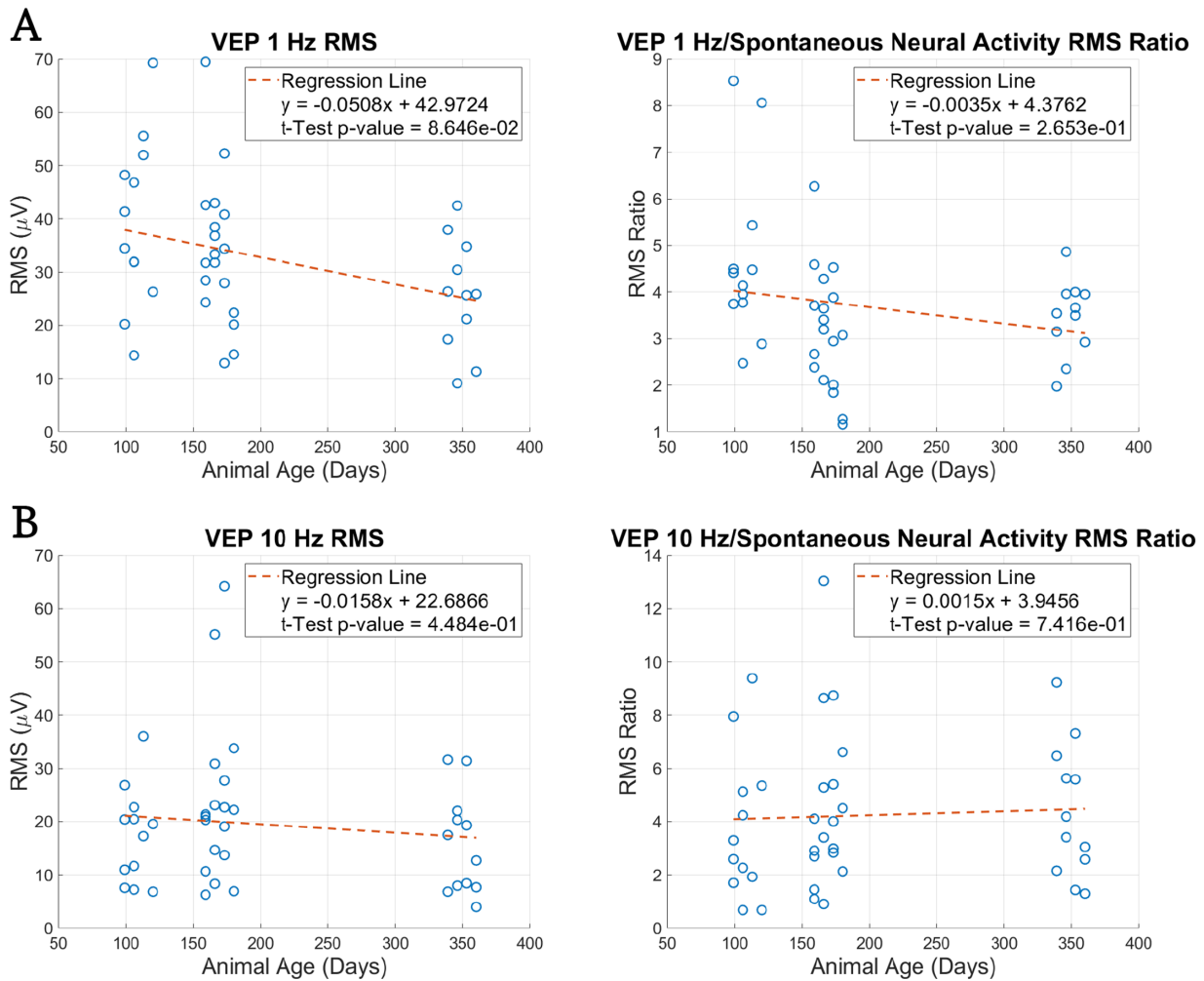


**Figure 9.** Plotted linear regression of RMS for (A) 1 Hz VEPs RMS and RMS ratio (B) 10 Hz VEPs RMS and RMS ratio. Statistical  $\alpha = 5.0e^{-02}$  for significance.

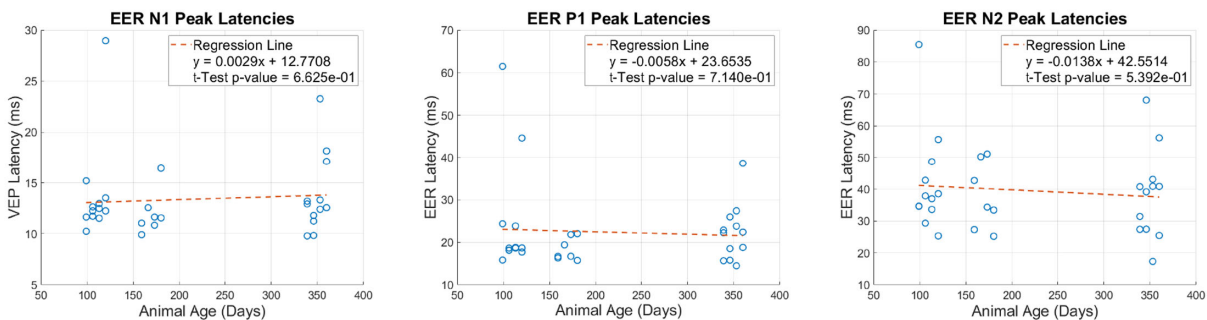


**Figure 10.** Plotted linear regression of EER peak latency for N1, P1, and N2 peaks. Statistical  $\alpha = 5.0e^{-02}$  for significance.

## Discussion

Retinal and cortical reorganization has been documented in response to retinal degeneration. Retinal changes include rewiring of retinal circuits<sup>40</sup> and transient increases in spontaneous activity.<sup>41</sup> The

ONL degeneration found in LE-P23H-1 through OCT is consistent with earlier studies of this model,<sup>21,24,34</sup> which correlates with a reduction in ERG response amplitude and an increase in b-wave latency. In the visual cortex, both functional and structural alterations have been found as a consequence of retinal degeneration.<sup>15,16,18,19</sup> Here, we assess the cortical response

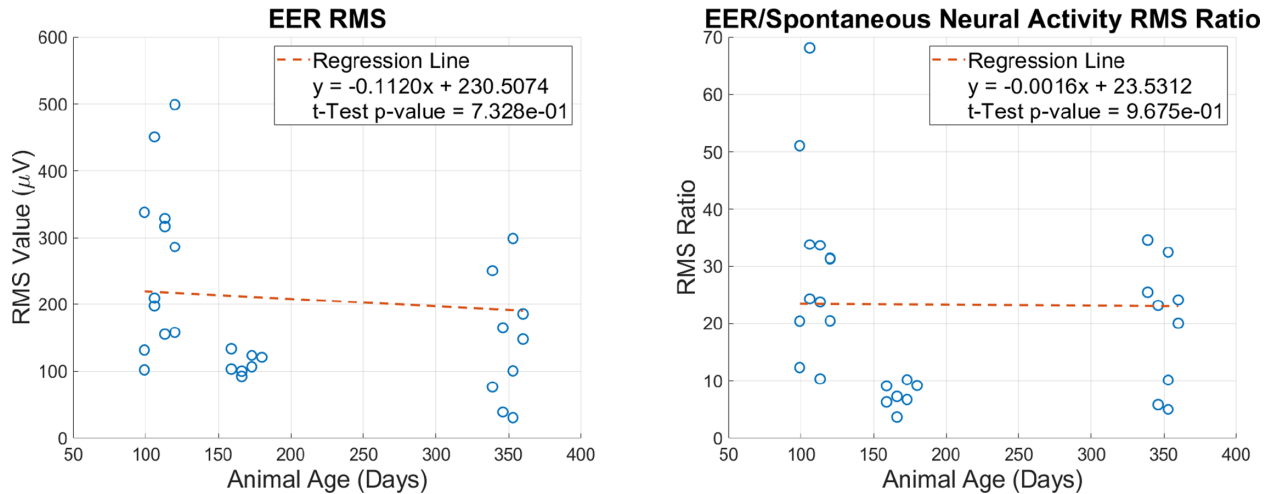


**Figure 11.** Plotted linear regression of EER RMS and RMS ratio. Statistical  $\alpha = 5.0e-2$  for significance.

to retinal stimulation as it related to animal age, and extent of retinal degeneration in a well-studied model of retinal degeneration.

OCT scans of LE-P23H-1 rats are consistent with prior studies of the retinal degeneration model. Our animals experienced a complete degeneration of the ONL, IS, and OS layers after P360. In our data, the IS layer thickness in P120 is larger than the IS layer in the Long-Evans group. This may be due to reduced visibility (at P120) of the OS reflectance used to differentiate the IS and OS, which resulted in layer thickness including both the IS and OS for this group. Heterogeneous expression of P23H in pigmented animals slowed photoreceptor degeneration, where complete degeneration by P180 was noted when P23H was cross bred with albino Sprague Dawley rats.<sup>21,24</sup> Albinism has been shown to exacerbate photoreceptor degeneration in mouse models.<sup>42</sup>

The increase in implicit time in the VEP is consistent with earlier studies of electrophysiology in P23H rat. LaVail et al. showed that implicit time of both scotopic and photopic b-wave was increased after 6 to 7 months of degeneration by approximately 10 to 20 ms, compared to 3-month measurements.<sup>24</sup> Although the age groups do not match ours, as they did not include a 12-month group, the delay noted in the ERG suggests that the N1 VEP delays we reported may be entirely due to dysfunction in the retina. For example, N1 10 Hz VEP increased by 20 ms for P360 versus P120, an increase that may be due to increased ERG latency. This bolsters our claim that a lack in EER implicit time differences with age indicates integrity of the optic nerve and cortical processing, despite severe retinal degeneration in P23H.

### Electric Stimulation and Retina Condition

Retinal degeneration had no measurable effect on EER peak latency and signal strength (as measured using RMS). EER peak latency values were comparable to epiretinal stimulation<sup>31</sup> and subretinal stimulation.<sup>33</sup> EER waveforms shown in Nimmagadda et al. have a similar time course as the EER we present, with the initial peak occurring near 17 ms in S334ter rats.<sup>31</sup> The latency discrepancy may be due to the lower level of stimulus amplitudes used in Nimmagadda et al. compared to our work.<sup>23</sup> The 100 µA used in Nimmagadda et al.<sup>23</sup> was chosen with intent to activate local stimulation to measure retinotopy in V1.<sup>23</sup> (Mandel et al.)<sup>33</sup> had an average of approximately 18 ms for N1 in RCS rats (average age = P79) compared to our average N1 of 12.44 ms. The latency discrepancy may be due to either the low stimulus amplitude or the target of stimulation. Mandel et al. used a subretinal implant, using photovoltaic energy transfer to stimulate the target tissue.<sup>33</sup> The subretinal implant specifically targets bipolar cells (using a small estimated 12 µA of stimulation current),<sup>27</sup> whereas corneal or epiretinal stimulation used in our experiments evokes responses in both retinal ganglion cells and bipolar cells. By targeting bipolar cells, a delay may occur from retinal processing between the bipolar cells and RGC layers. Although the modality of stimulation varied from corneal, epiretinal, and subretinal stimulation, electric stimulation of the retina activated V1 with comparable latency, which supports our claim that corneal stimulation evokes activity in the retina. Human studies have also established that corneal stimulation activates the retina.<sup>43</sup>

Weekly and biweekly corneal electric stimulation did not induce corneal damage or cataracts after 4-weeks of stimulation. Animals that received weekly electric stimulation still had detectable VEP waveforms at week 4. These findings are consistent with the Okuvision clinical trials where repeated use of TES was found to be safe.<sup>6-9</sup>

Electric stimulation can activate neural plasticity mechanisms (dendrite sprouting and long-term potentiation) and is used for understanding neuroplasticity in neuroscience.<sup>44-46</sup> One hypothesis we sought to test is that regular electrical stimulation will increase the efficiency of visual processing in retinal degeneration, as reflected by reduced VEP latency and increased VEP amplitude. This hypothesis was based on findings of improved retinal condition after therapeutic electrical stimulation. However, we found no effect of electric stimulation on VEP latency or amplitude after 4 weeks. There are several reasons why VEP may remain unchanged in our experiments, in spite of corneal stimulation. Changes noted in the retina in other corneal stimulation experiments, such as increased RGC count,<sup>10</sup> may not have affected VEP properties in a significant manner. The VEP measurements using 1 mm diameter screws may not be sensitive to small changes in retinal or cortical signaling, because it is a gross measurement of cortical activity. The 4-week time period may not have been adequate to demonstrate an effect on VEP waveforms, because we noted increase in latency in animal groups separated by 3 to 6 months. Future studies should extend the length of TES to assess its effect on VEP.

### Applicability to Vision Health Assessments

Clinical electrophysiology typically uses light stimulation to assess the health of the visual system. These same measurements are frequently used in preclinical research. Multifocal ERG and multifocal VEP measurements offer spatially discrete assessment of central and peripheral vision health. In turn, dysfunction in the photoreceptors eliminates the ability to assess other parts of the visual pathways. EER may be a useful and complementary technique to verify the health of RGCs, optic nerve, and downstream visual pathways, bypassing the retina's light transduction requirements. Optic nerve damage, typical of blunt trauma, of glaucoma, or of neuroinflammatory diseases, may be assessed more directly using electric stimulation as the stimuli source.

Management of eye disease requires better assessment of the eye's functional and metabolic condition. In the case of diabetes, neurodegeneration of the retina may occur before clinically appreciated diabetic

retinopathy.<sup>47</sup> Those affected by diabetes report poorer vision even before the outstanding markers, angiogenesis, and macular edema, of diabetic retinopathy are apparent. EER may offer additional information to aid diagnosis of the visual processing circuit's condition. EER recordings, using scalp electrodes, have been successfully derived from corneal electric stimulation in humans.<sup>43</sup> Multichannel corneal stimulations that can focus stimulation in a single retinal quadrant adds to the utility of EER as a diagnostic tool,<sup>48</sup> and coupling focuses retinal stimulation with electro-encephalograph (EEG) recording characterize spatial differences in visual pathway condition. Refined methods of electric stimulation artifact removal with multitrial averaging,<sup>38</sup> model artifact subtraction,<sup>49</sup> and hardware considerations to preventing artifact from transient current injection<sup>50,51</sup> allow for easier extract of event-related neural signals with higher quality. Having patients report the location and nature of their perceptions can confirm focal retinal activation and complement EEG data.

### Limitations

Our work used recording screws to target a general stereotaxic location to record responses from full-field light and electric stimulation. These gross measurements using the recording screws likely limited our ability to detect subtle changes in neural signals. Multichannel recording implants can provide more information, but these implants are known to alter the cortical tissue significantly and lose the ability to record signals over time. These time-related changes in signal stability will confound an experiment that seeks to track over time changes due to retinal degeneration. Optical recording from cortical neurons has improved dramatically in recent years, but latency is difficult to record with optical methods. Improved neural recording devices that remain stable with time may allow long-term studies that do not cause cortical modification.<sup>52,53</sup>

EER recordings required artifact removal, which relies on accompanying assumptions about the stimulated eye and brain complex. Blanking the recording -1 to 5 ms at the stimulation event assumed no evoked neural response during that time period. The minimum response time from the retinal ganglion to the optic nerve using electric stimulation is reported to be 3 ms.<sup>54</sup> Considering the optic nerve's downstream connections of the LGN prior to V1, the remaining 2 ms of the blanking window should not include any neural activity. The artifact subtraction with the 5% isoflurane recording assumes that electric conductivity, from the cornea to the recording screws, was relatively consistent

between the weekly trials. As the 5% isoflurane application should mute all neural activity and response, the only remaining content of the EER recording after subtraction should be the EER event with spontaneous oscillations. Even so, artifact removal in application alters the objective EER RMS, because some artifact is included in the RMS calculation.

## Conclusion

Cortical evoked potential recording of the retinal degenerate rat model shows that light and electric stimulation data are readily available to provide information on the visual pathways in this model. Comparison of VEP recording shows that retinal degeneration changes V1 neural function. In contrast, EER remains relatively preserved compared to VEP, allowing for assay of visual neural circuit that circumvents photoreceptor activation requirement affected by retinal degeneration.

## Acknowledgments

The authors thank Elissa Welle and Paras Patel for providing the printed circuit board design for the cortical recording device and Chris Andrews for consultation on linear mixed models. Andrews' contribution was supported by the National Institute of Neurological Disorders and Stroke of the National Institutes of Health under Award Number T32NS115724. The content is solely the responsibility of the authors and does not necessarily represent the official views of the National Institutes of Health.

Also supported by the University of Michigan College of Engineering and the School of Medicine, and National Science Foundation Award INSPiRE 1343193.

Financial Disclosure Statement: J.D.W. has a research collaboration with Second Sight Medical Products, Inc.

Disclosure: **B. Koo**, None; **J.D. Weiland**, None

## References

1. Scott AW, Bressler NM, Ffolkes S, Wittenborn JS, Jorkasky J. Public Attitudes About Eye and Vision Health. *JAMA Ophthalmol.* 2016;134(10):1111–1118.
2. Hartong DT, Berson EL, Dryja TP. Retinitis pigmentosa. *The Lancet.* 2006;368(9549):1795–1809.
3. Weiland JD, Humayun MS. Retinal Prosthesis. *IEEE Trans Biomed Engineer.* 2014;61(5):1412–1424.
4. da Cruz L, Dorn JD, Humayun MS, et al. Five-Year Safety and Performance Results from the Argus II Retinal Prosthesis System Clinical Trial. *Ophthalmology.* 2016;123(10):2248–2254.
5. Duncan JL, Richards TP, Arditi A, et al. Improvements in vision-related quality of life in blind patients implanted with the Argus II Epiretinal Prosthesis. *Clin Exp Optom.* 2017;100(2):144–150.
6. Jolly JK, Wagner SK, Martus P, et al. Transcorneal Electrical Stimulation for the Treatment of Retinitis Pigmentosa: A Multicenter Safety Study of the OkuStim System (TESOLA-Study). *Ophthalmic Res.* 2020;63:234–243.
7. Sinim Kahraman N, Oner A. Effect of Transcorneal Electrical Stimulation on Patients with Retinitis Pigmentosa. *J Ocul Pharmacol Ther.* 2020;36(8):609–617.
8. Schatz A, Pach J, Gosheva M, et al. Transcorneal Electrical Stimulation for Patients With Retinitis Pigmentosa: A Prospective, Randomized, Sham-Controlled Follow-up Study Over 1 Year. *Invest Ophthalmol Vis Sci.* 2017;58(1):257–269.
9. Bittner AK, Seger K. Longevity of visual improvements following transcorneal electrical stimulation and efficacy of retreatment in three individuals with retinitis pigmentosa. *Graefes Arch Clin Exp Ophthalmol.* 2018;256(2):299–306.
10. Hanif AM, Kim MK, Thomas JG, et al. Whole-eye electrical stimulation therapy preserves visual function and structure in P23H-1 rats. *Exp Eye Res.* 2016;149:75–83.
11. Morimoto T, Fujikado T, Choi J-S, et al. Transcorneal Electrical Stimulation Promotes the Survival of Photoreceptors and Preserves Retinal Function in Royal College of Surgeons Rats. *Invest Ophthalmol Vis Sci.* 2007;48(10):4725–4732.
12. Pardue MT, Phillips MJ, Yin H, et al. Neuroprotective Effect of Subretinal Implants in the RCS Rat. *Invest Ophthalmol Vis Sci.* 2005;46(2):674–682.
13. Lou AR, Madsen KH, Julian HO, et al. Postoperative increase in grey matter volume in visual cortex after unilateral cataract surgery. *Acta Ophthalmol.* 2013;91(1):58–65.
14. Lin H, Zhang L, Lin D, et al. Visual Restoration after Cataract Surgery Promotes Functional and Structural Brain Recovery. *EBioMedicine.* 2018;30:52–61.

15. Castaldi E, Cicchini GM, Cinelli L, Biagi L, Rizzo S, Morrone MC. Visual BOLD Response in Late Blind Subjects with Argus II Retinal Prosthesis. *PLoS Biology*. 2016;14(10):e1002569.
16. Abbasi B, Rizzo JF. Advances in Neuroscience, Not Devices, Will Determine the Effectiveness of Visual Prostheses. *Seminars Ophthalmol*. 2021;36(4):168–175.
17. Ferreira S, Pereira AC, Quendera B, Reis A, Silva ED, Castelo-Branco M. Primary visual cortical remapping in patients with inherited peripheral retinal degeneration. *NeuroImage: Clinical*. 2017;13:428–438.
18. Cunningham SI, Weiland JD, Bao P, Lopez-Jaime GR, Tjan BS. Correlation of vision loss with tactile-evoked V1 responses in retinitis pigmentosa. *Vis Res*. 2015;111:197–207.
19. Dan H-D, Zhou F-Q, Huang X, Xing Y-Q, Shen Y. Altered intra- and inter-regional functional connectivity of the visual cortex in individuals with peripheral vision loss due to retinitis pigmentosa. *Vis Res*. 2019;159:68–75.
20. Morimoto T, Fujikado T, Choi J-S, et al. Transcorneal Electrical Stimulation Promotes the Survival of Photoreceptors and Preserves Retinal Function in Royal College of Surgeons Rats. *Invest Ophthalmol Vis Sci*. 2007;48(10):4725–4732.
21. Orhan E, Dalkara D, Neullé M, et al. Genotypic and Phenotypic Characterization of P23H Line 1 Rat Model. *PLoS One*. 2015;10(5):e0127319.
22. Wang Y, Chen K, Xu P, Ng TK, Chan LLH. Spontaneous neural activity in the primary visual cortex of retinal degenerated rats. *Neurosci Lett*. 2016;623:42–46.
23. Nimmagadda K, Weiland JD. Retinotopic Responses in the Visual Cortex Elicited by Epiretinal Electrical Stimulation in Normal and Retinal Degenerate Rats. *Transl Vis Sci Technol*. 2018;7(5):33.
24. LaVail MM, Nishikawa S, Steinberg RH, et al. Phenotypic characterization of P23H and S334ter rhodopsin transgenic rat models of inherited retinal degeneration. *Exp Eye Res*. 2018;167:56–90.
25. Sohocki MM, Daiger SP, Bowne SJ, et al. Prevalence of mutations causing retinitis pigmentosa and other inherited retinopathies. *Hum Mutat*. 2001;17(1):42–51.
26. Sung CH, Davenport CM, Hennessey JC, et al. Rhodopsin mutations in autosomal dominant retinitis pigmentosa. *Proc Natl Acad Sci USA*. 1991;88(15):6481–6485.
27. Wang L, Mathieson K, Kamins TI, et al. Photo-voltaic retinal prosthesis: implant fabrication and performance. *J Neural Eng*. 2012;9(4):046014.
28. Greco JA, Wagner NL, Jensen RJ, et al. Activation of retinal ganglion cells using a biomimetic artificial retina. *J Neural Eng*. 2021;18(6):066027.
29. Nguyen D, Valet M, Dégardin J, et al. Novel Graphene Electrode for Retinal Implants: An in vivo Biocompatibility Study. *Front Neurosci*. 2021;15:615256.
30. Salzmann J, Linderholm OP, Guyomard J-L, et al. Subretinal electrode implantation in the P23H rat for chronic stimulations. *Br J Ophthalmol*. 2006;90(9):1183–1187.
31. Weiland JD, Fujii GY, Tameesh MK, et al. Chronic electrical stimulation of the canine retina. *Proceedings of the Second Joint 24th Annual Conference and the Annual Fall Meeting of the Biomedical Engineering Society [Engineering in Medicine and Biology]*, 2002. 3:2051–2052.
32. Maya-Vetencourt JF, Ghezzi D, Antognazza MR, et al. A fully organic retinal prosthesis restores vision in a rat model of degenerative blindness. *Nature Mater*. 2017;16(6):681–689.
33. Mandel Y, Goetz G, Lavinsky D, et al. Cortical responses elicited by photovoltaic subretinal prostheses exhibit similarities to visually evoked potentials. *Nat Commun*. 2013;4(1):1980.
34. Parisi V, Ziccardi L, Stifano G, Montrone L, Galinaro G, Falsini B. Impact of regional retinal responses on cortical visually evoked responses: Multifocal ERGs and VEPs in the retinitis pigmentosa model. *Clin Neurophysiol*. 2010;121(3):380–385.
35. Schindelin J, Arganda-Carreras I, Frise E, et al. Fiji: an open-source platform for biological-image analysis. *Nat Methods*. 2012;9(7):676–682.
36. Berger A, Cavallero S, Dominguez E, et al. Spectral-Domain Optical Coherence Tomography of the Rodent Eye: Highlighting Layers of the Outer Retina Using Signal Averaging and Comparison with Histology. *PLoS One*. 2014;9(5):e96494.
37. Monai N, Yamauchi K, Tanabu R, Gonome T, Ishiguro S, Nakazawa M. Characterization of photoreceptor degeneration in the rhodopsin P23H transgenic rat line 2 using optical coherence tomography. *PLoS One*. 2018;13(3):e0193778.
38. Takahashi S, Anzai Y, Sakurai Y. A new approach to spike sorting for multi-neuronal activities recorded with a tetrode—how ICA can be practical. *Neurosci Res*. 2003;46(3):265–272.
39. Nason SR, Vaskov AK, Willsey MS, et al. A low-power band of neuronal spiking activity dominated by local single units improves the performance of brain-machine interfaces. *Nat Biomed Eng*. 2020;4(10):973–983.

40. Jones BW, Watt CB, Marc RE. Retinal remodeling. *Clin Exp Optom*. 2005;88(5):282–291.
41. Trenholm S, Awatramani GB. Origins of spontaneous activity in the degenerating retina. *Front Cell Neurosci*. 2015;9:277.
42. Naash MI, Ripps H, Li S, Goto Y, Peachey NS. Polygenic disease and retinitis pigmentosa: albinism exacerbates photoreceptor degeneration induced by the expression of a mutant opsin in transgenic mice. *J Neurosci*. 1996;16(24):7853–7858.
43. Potts AM, Inoue J, Buffum D. The Electrically Evoked Response of the Visual System (EER). *Invest Ophthalmol Vis Sci*. 1968;7(3):269–278.
44. Begenisic T, Mazziotti R, Sagona G, et al. Preservation of Visual Cortex Plasticity in Retinitis Pigmentosa. *Neuroscience*. 2020;424:205–210.
45. Lunghi C, Galli-Resta L, Binda P, et al. Visual Cortical Plasticity in Retinitis Pigmentosa. *Invest Ophthalmol Vis Sci*. 2019;60(7):2753–2763.
46. Cheng X, Li T, Zhou H, et al. Cortical electrical stimulation with varied low frequencies promotes functional recovery and brain remodeling in a rat model of ischemia. *Brain Res Bull*. 2012;89(3):124–132.
47. Simó R, Stitt AW, Gardner TW. Neurodegeneration in diabetic retinopathy: does it really matter? *Diabetologia*. 2018;61(9):1902–1912.
48. Lee S, Park J, Kwon J, Kim DH, Im C-H. Multi-channel transorbital electrical stimulation for effective stimulation of posterior retina. *Sci Rep*. 2021;11(1):9745.
49. Hashimoto T, Elder CM, Vitek JL. A template subtraction method for stimulus artifact removal in high-frequency deep brain stimulation. *J Neurosci Meth*. 2002;113(2):181–186.
50. Liu X, Li J, Chen T, Wang W, Je M. A Neural Recording and Stimulation Chip with Artifact Suppression for Biomedical Devices. *J Healthcare Eng*. 2021;2021:e4153155.
51. Li J, Liu X, Mao W, Chen T, Yu H. Advances in Neural Recording and Stimulation Integrated Circuits. *Front Neurosci*. 2021;15:663204.
52. Patel PR, Zhang H, Robbins MT, et al. Chronic in vivo stability assessment of carbon fiber microelectrode arrays. *J Neural Eng*. 2016;13(6):066002.
53. Welle EJ, Patel PR, Woods JE, et al. Ultra-small carbon fiber electrode recording site optimization and improved in vivo chronic recording yield. *J Neural Eng*. 2020;17(2):026037.
54. O’Hearn TM, Sadda SR, Weiland JD, Maia M, Margalit E, Humayun MS. Electrical stimulation in normal and retinal degeneration (rd1) isolated mouse retina. *Vis Res*. 2006;46(19):3198–3204.